Trifluoperazine, a Well-Known Antipsychotic, Inhibits Glioblastoma Invasion by Binding to Calmodulin and Disinhibiting Calcium Release Channel IP₃R

Seokmin Kang[1], Jinpyo Hong[2], Jung Moo Lee[2,3], Hyo Eun Moon[4], Borami Jeon[5,6], Jungil Choi[7], Nal Ae Yoon[1], Sun Ha Paek[4], Eun Joo Roh[5,6], C. Justin Lee[2,3,8], and Sang Soo Kang[1]

Abstract

Calcium (Ca^{2+}) signaling is an important signaling process, implicated in cancer cell proliferation and motility of the deadly glioblastomas that aggressively invade neighboring brain tissue. We have previously demonstrated that caffeine blocks glioblastoma invasion and extends survival by inhibiting Ca^{2+} release channel inositol 1,4,5-trisphosphate receptor (IP₃R) subtype 3. Trifluoperazine (TFP) is an FDA-approved antipsychotic drug for schizophrenia. Interestingly, TFP has been recently reported to show a strong anticancer effect on lung cancer, hepatocellular carcinoma, and T-cell lymphoma. However, the possible anticancer effect of TFP on glioblastoma has not been tested. Here, we report that TFP potently suppresses proliferation, motility, and invasion of glioblastoma cells *in vitro*, and tumor growth in *in vivo* xenograft mouse model. Unlike caffeine, TFP triggers massive and irreversible release of Ca^{2+} from intracellular stores by IP₃R subtype 1 and 2 by directly interacting at the TFP-binding site of a Ca^{2+}-binding protein, calmodulin subtype 2 (CaM2). TFP binding to CaM2 causes a dissociation of CaM2 from IP₃R and subsequent opening of IP₃R. Compared with the control neural stem cells, various glioblastoma cell lines showed enhanced expression of CaM2 and thus enhanced sensitivity to TFP. On the basis of these findings, we propose TFP as a potential therapeutic drug for glioblastoma by aberrantly and irreversibly increasing Ca^{2+} in glioblastoma cells. *Mol Cancer Ther; 16(1); 217–27. ©2016 AACR.*

Introduction

Glioblastoma is the most common and aggressive malignant primary brain tumor, accounting for more than 50% of all brain tumor cases. Moreover, glioblastoma has a very poor prognosis, with a less than 5% 5-year survival rate and a median survival time of 1 year (1–4). Standard therapy of glioblastoma consists of a surgical resection of glioblastoma and adjuvant therapy with anticancer drug, such as the alkylating agent temozolomide. However, a complete surgical resection is almost impossible due to aggressive invasion of glioblastoma over time throughout the brain (5). In addition, temozolomide provides only modest benefits and increases the patients' life expectancy merely by about 2.5 months, with tumor relapse frequently observed (6, 7). Therefore, there is a pressing need for finding more effective anticancer therapy for glioblastoma.

Interestingly, some commonly used antipsychotic drugs show antiproliferative effect (8) and have been recently proposed as anticancer drugs. A recent study showed that patients with schizophrenia are not only less susceptible to cancer (1.93%) than non-schizophrenic controls (2.97%) during a 9-year follow-up period (9), but also some psychotropic agents, including antipsychotics, antidepressants, and mood stabilizers, possess a significant *in vitro* antiproliferative activity (10, 11). For example, trifluoperazine (TFP), which is an FDA-approved antipsychotic and antiemetic drug (12) used for treating schizophrenia (13), has been shown to inhibit cell proliferation and invasion and to induce cell death in several types of cancer cell lines and animal models (14–21). However, whether TFP has any anticancer effect in glioblastoma has not been investigated.

One of the proposed modes of action of TFP is its ability to bind to a well-known Ca^{2+}-binding protein, calmodulin (CaM). It has been reported that TFP exerts an inhibitory action on the function of CaM by directly binding to CaM (22). In particular, CaM is

[1]Department of Anatomy and Convergence Medical Science, Institute of Health Sciences, School of Medicine, Gyeongsang National University, Jinju, Republic of Korea. [2]Center for Neuroscience and Functional Connectomics, Brain Science Institute, Korea Institute of Science and Technology, Seoul, Republic of Korea. [3]KU-KIST Graduate School of Converging Science and Technology, Korea University, Seoul, Republic of Korea. [4]Department of Neurosurgery, Seoul National University College of Medicine, Seoul, Republic of Korea. [5]Chemical Kinomics Research Center, Korea Institute of Science and Technology, Seoul, Republic of Korea. [6]Department of Biological Chemistry, Korea University of Science and Technology, Daejeon, Republic of Korea. [7]Gyeongnam Department of Environmental Toxicology and Chemistry, Korea Institute of Toxicology, Jinju, Republic of Korea. [8]Neuroscience Program, University of Science and Technology, Daejeon, Republic of Korea.

Note: Supplementary data for this article are available at Molecular Cancer Therapeutics Online (http://mct.aacrjournals.org/).

S. Kang, J. Hong, and J.M. Lee contributed equally to this article.

Corresponding Authors: Sang Soo Kang, Department of Anatomy and Convergence Medical Science, Gyeongsang National University, 15 Jinju-daero 816 Beon-gil, Jinju, Gyeongsangnam-do 52727, Republic of Korea (South). Phone: 825-5772-8033; Fax: 825-5772-8039; E-mail: Kangss@gnu.ac.kr; and C. Justin Lee, Center for Neuroscience and Functional Connectomics, Brain Science Institute, Korea Institute of Science and Technology, 5, Hwarang-ro 14-gil, Seongbuk-gu, Seoul 02792, Republic of Korea. Phone: 822-958-6940; Fax: 822-958-6937; E-mail: cjl@kist.re.kr

doi: 10.1158/1535-7163.MCT-16-0169-T

known to interact with inositol 1,4,5-trisphosphate receptor (IP$_3$R), which is a Ca^{2+} release channel located on intracellular Ca^{2+} stores, such as endoplasmic reticulum (23). IP$_3$R is a tetrameric protein, and each of its subunits consists of an N-terminal ligand-binding domain, a C-terminal transmembrane pore domain, and an intervening modulatory domain (24). It is well known that the opening of IP$_3$R is regulated by both IP$_3$ and Ca^{2+} (24). When Ca^{2+} binds to CaM, the Ca^{2+}/CaM complex can interact with N-terminal ligand-binding domain of IP$_3$R, causing it to inhibit IP$_3$R (24, 25). Therefore, it is possible that TFP binding to CaM might have a profound effect on IP$_3$R channel function and IP$_3$R-mediated Ca^{2+} release. However, this possibility has not been tested yet.

Ca^{2+} is one of the crucial molecules involved in intracellular signaling, which is important for cell proliferation, and survival (5, 26). When it comes to glioblastoma, Ca^{2+} signaling is critical for proliferation, migration, and invasion (27). We previously reported that caffeine blocks an increase in intracellular Ca^{2+} concentration, which is caused by the signaling of several G-protein–coupled receptors, in glioblastoma cells by inhibition of Ca^{2+} release channel IP$_3$R subtype 3 (5). As a result, caffeine suppresses glioblastoma cells proliferation, migration, and invasion and extends survival in animal models (5). From that study, we proposed that targeting Ca^{2+} signaling can be a valuable therapeutic target for treating glioblastoma.

In the current study, we investigated whether TFP could inhibit glioblastoma proliferation and invasion by targeting Ca^{2+} signaling. We found that, unlike caffeine, TFP binding to CaM2 increased intracellular Ca^{2+} release through opening of IP$_3$R subtype 1 and 2 by causing a dissociation of CaM2 from IP$_3$R. Through this mechanism, TFP suppressed the proliferation, motility, and invasion of glioblastoma cells in *in vitro* and *in vivo* xenograft model.

Materials and Methods

Cells lines and culture

U87MG human glioblastoma cells were obtained from the ATCC in 2006. Human primary glioblastoma (GBL) cell lines (GBL12, GBL13, GBL14, GBL15, GBL28, GBL30, GBL227, and GBL232) and neural stem cells (NSC) were generated from the Seoul National University Hospital (Seoul, Korea, IRB nr.; H-0507-509-153). All cell lines originated from the human neuronal system. All cells were cultured in 5% CO$_2$ and air humidified in a 37°C incubator. Culture media were DMEM (Corning Costar) containing 10% FBS, 100 U/mL penicillin, and 100 µg/mL streptomycin (Gibco Invitrogen). Each cell line at early passages was stocked, and cultures were maintained until passage 20 (within 2 months).

Tumor cell viability

Cells were seeded into 96-well plates at a density of 1.5×10^3 cells per well and allowed to attach for 24 hours. Cells were treated with vehicle or the indicated concentrations of TFP (Sigma) diluted in complete media for each 24, 48, and 72 hours. Cell proliferation was determined by 3-[4, 5-dimethylthiazol-2-yl]-2, 5-diphenyltetrazolium bromide (MTT) assay. At the end of the TFP treatment, 100 µL of 1× MTT (Amresco) labeling reagent was added to each well and incubated for another 2 hours. The proliferative activities were expressed as the relative percentage of cell numbers at initial time.

Anchorage-independent cell growth

Cells per well (5×10^4) were seeded in 0.3% cell agar layer, which was on top of 0.6% base agar layer in 6-well culture plates. The solidified cell layer was covered with the medium containing TFP, which was replaced every 4 days. Cells were then incubated for a further 2 weeks at 37°C and 5% CO$_2$. Afterward, colonies were stained with 0.05% cresyl violet and photographed.

Matrigel invasion assay

Cell invasion was assayed as described previously (5). The mean number of untreated cells was considered as 100% invasion. Each condition was triplicated, and five fields were randomly selected and counted for each assay. TFP was added at the time of cell plating.

Animal study with skin and brain xenograft

In the skin xenograft model, 5-week-old athymic mice (BALB/c nu/nu) were obtained from Central Laboratory Animal, Inc. For the xenograft tumor growth assay, U87MG cells (150 µL; 3×10^6 cells) were subcutaneously injected into the right flanks of the mice. On the third day after injection, TFP was given as an intraperitoneal injection (5 mg/kg/day). The control animals were given 0.9% saline. A total of 21 days treatments were given, with a 24-hour rest period. Athymic mice (BALB/c nu/nu) bearing U87MG cells were randomized into two groups (control and TFP; $n = 5$ per group) when the volume of tumor reached 40 mm^3. Tumor volume and body weight were measured daily for 21 days with a caliper and electronic balance. Tumor volumes were calculated by the following formula: volume = length × width^2/2. After 21 days, all animals were euthanized and autopsied. Tumors and lung organs were collected and fixed by 4% paraformaldehyde in PBS.

In the brain xenograft model, an orthotopic implantation model was established with same cell line. U87MG cells (5 µL; 2.5×10^5 cells) were implanted by intracranial injections in the left frontal lobe at coordinates 2 mm lateral from the bregma, 0.5 mm anterior, and 3.5 mm intraparenchymal. TFP (10 mg/kg/day) was given as an intraperitoneal injection 3 days after implantation and drug administration schedule was same as flank xenograft model. Mice were monitored daily for general appearance, behavioral changes, and neurologic deficits. Mice were sacrificed when moribund. All protocols were approved by the Gyeongsang National University Institutional Animal Care and Use Committee.

Histology

Mouse lung and brain tissues were stained with hematoxylin and eosin (H&E). For H&E staining, the fixed tumors were embedded in paraffin, cut into 5 µm sections, and stained with H&E. Slides were photographed using an optical or confocal microscope (BX61VS, Olympus).

Infection of *IP$_3$R* and *CaM* shRNA

Before replating onto a cover glass for calcium imaging and Western blotting, lentivirus carrying scrambled shRNA or *IP$_3$R* subtype 1, 2, 3 shRNA or *CaM* shRNA was infected to cultured U87MG cells or GBL28 cells seeded on 35- or 60-mm dishes. Each shRNA sequence for each *IP$_3$R* subtype and *CaM* is described in Supplementary Table S1.

Ca²⁺ imaging

Ca^{2+} imaging was performed as described previously (5). Intensity images of 510 nm wavelength were taken at 340 and 380 nm excitation wavelengths using either iXon EMCCD (DV887 DCS-BV, ANDOR Technology). The two resulting images were used for ratio calculations in Axon Imaging Workbench version 6.2 (Axon Instruments).

qRT-PCR

qRT-PCR was done by using SYBR Green PCR Master Mix. Reactions were performed in duplicates in a total volume of 10 μL containing 10 pmol/L primer, 4 μL cDNA, and 5 μL SYBR Green PCR Master Mix (Applied Biosystems). The mRNA level of *CaM* subtypes was normalized to that of *GAPDH* mRNA. Fold induction was calculated using the $2^{-\Delta\Delta C_t}$ method. The following sequences of primers were used for real-time RT-PCR. *CaM* primer sequences were as follows: GAPDH_Fwd 5′-AGCTGAACGGGAA-GCTCA-3′; GAPDH_Rev 5′-TGCTGTAGCCAAATTCGT-3′; *calmodulin1*_Fwd: 5′-ACTGGGTCAGAACCCAACAG-3′; *calmodulin1*_ Rev: 5′-TGCCTCACGGATTTCTTCTT-3′; *calmodulin2*_Fwd: 5′-ATGCTGATGGTAATGGCACA-3′; *calmodulin2*_Rev: 5′–TGT-CATCACATGGCGAAGTT-3′; *calmodulin3*_Fwd: 5′–GATGAGAT-CCCTGGGACAGA-3′; *calmodulin3*_Rev: 5′–CTCGGATCTCC-TCCTCACTG-3′.

Real-time cell migration

Cell Observer (Carl Zeiss) was used to observe real-time glioblastoma behavior pattern in TFP-treated medium. Cells were seeded at 1×10^4 cells per well on 12-well plates and cultured overnight. Cells were treated with TFP in medium under standard cell culture conditions. Cultured cells in the medium without adding TFP were taken as a control. After 4 hours, culture plates were transferred to the Cell Observer and maintained at 37°C in 5% CO_2. Images were captured at 5-minute intervals for 25 hours. The recorded images were analyzed by supported software (Axio Vision, Carl Zeiss) to determine motility for each sample.

Western blot and protein quantification

U87MG cells were lysed with RIPA buffer (Thermo Fisher Scientific). Total protein concentrations were determined using BCA assay (Thermo Fisher Scientific). An equal volume of 4× SDS sample buffer was added, and the samples were boiled for 5 minutes. Equivalent amounts of total protein (20–30 μg) were separated by SDS-PAGE on 4% to 10% polyacrylamide gel and then transferred to nitrocellulose membrane. The membrane was blocked with 5% skimmed milk or 3% BSA in 0.1% Tween-20/ Tris-buffered saline (TBS-T). The membrane was incubated with IP₃R1 (1:1,000, ab5804, Abcam), IP₃R2 (1:1,000, ab55981, Abcam), IP₃R3 (1:1,000, ab55983, Abcam), and β-actin (1:10,000, Thermo Fisher Scientific) antibodies overnight at 4°C.

Statistical analysis

When two groups were being compared, the significance of data was assessed by the two-tailed Student unpaired *t* test using Microsoft Excel software. Other statistical analyses were done using GraphPad Prism for Windows (Version 5.0, GraphPad Software). Differences between 3 or more means were determined by one-way ANOVA with Dunnett multiple comparison test. Linear mixed effects regression models were used to estimate and compare the group-specific change in tumor growth curves.

Differences in survival curves were determined by log-rank test. All statistical analyses were performed at the $P < 0.05$ level of significance.

Results

### The inhibitory effect of TFP on cultured glioblastoma cells

First, we investigated the effect of TFP on the cell viability of U87MG glioblastoma cells by MTT assay. We found that U87MG cell viability decreased time dependently (24, 48, and 72-hour TFP treatment) as well as dose dependently (1, 2, 5, 10, and 20 μmol/L of TFP; Fig. 1A), suggesting that TFP has a cytotoxic effect on glioblastoma cells.

To test the effect of TFP on anchorage-independent growth of U87MG glioblastoma cells, we performed colony formation assay. We observed that TFP significantly suppressed anchorage-independent growth at a concentration higher than 2 μmol/L (Fig. 1B). Because of the high invasive activity of glioblastoma cells in the brain tissue (6), we investigated the effect of TFP on invasion of U87MG cells by performing Matrigel transwell invasion assay (Fig. 1B). We observed that TFP significantly restricted the invasion of glioblastoma cells at a concentration higher than 1 μmol/L, with a half-maximal effective concentration at around 10 μmol/L (Fig. 1B). These results suggested that TFP potently inhibits colony formation and invasion of glioblastoma cells.

To investigate the effect on TFP on cellular morphology of U87MG cells, we performed live cell imaging and analysis (Supplementary movie S1). We observed dynamic changes in cellular morphology in U87MG cells during TFP treatment in a dose-dependent manner (5, 10, 15, 20, and 25 μmol/L; Supplementary Fig. S1A). The cellular morphology changed quickly in response to TFP, and eventually, most cells were detached from the plate and died after 25 hours (Supplementary Fig. S1A). Furthermore, the ratio of proliferated glioblastoma cells was significantly decreased in TFP-treated cells compared with 0.9% saline-treated cells as control (Supplementary Fig. S1B). These results were consistent with the results of MTT assay, suggesting that TFP potently induces glioblastoma cell death.

TFP inhibits glioblastoma growth and metastasis on *in vivo* xenograft model

To examine the *in vivo* effect of TFP, we transplanted U87MG cells subcutaneously into the athymic mice (BALB/c nu/nu) and checked tumor volume, weight, and lung tumor incidence during 21 days (Fig. 2A). We found that TFP treatment (5 mg/kg/day) significantly suppressed the glioblastoma growth of the xenograft mice as evidenced by a marked decrease of glioblastoma tumor size in TFP-treated mice at day 21 (Fig. 2A). Next, we monitored daily progression of the tumor volume during 21 days from the day of intraperitoneal injection of U87MG cells. We found that tumor volume of TFP-treated mice was significantly decreased compared with control mice without TFP starting from day 17 (Fig. 2B). Furthermore, tumor weight of TFP-treated mice was about 50% of control at day 21 (Fig. 2C). However, there was no difference between the mean bodyweights of the two groups over the same period (Supplementary Fig. S2). The lung is known to contain many blood and lymphatic vessels originating from various other organs and is prone to invasion of tumors from several other organs. Therefore, we measured whether TFP can inhibit lung metastasis in the skin xenograft model. The results
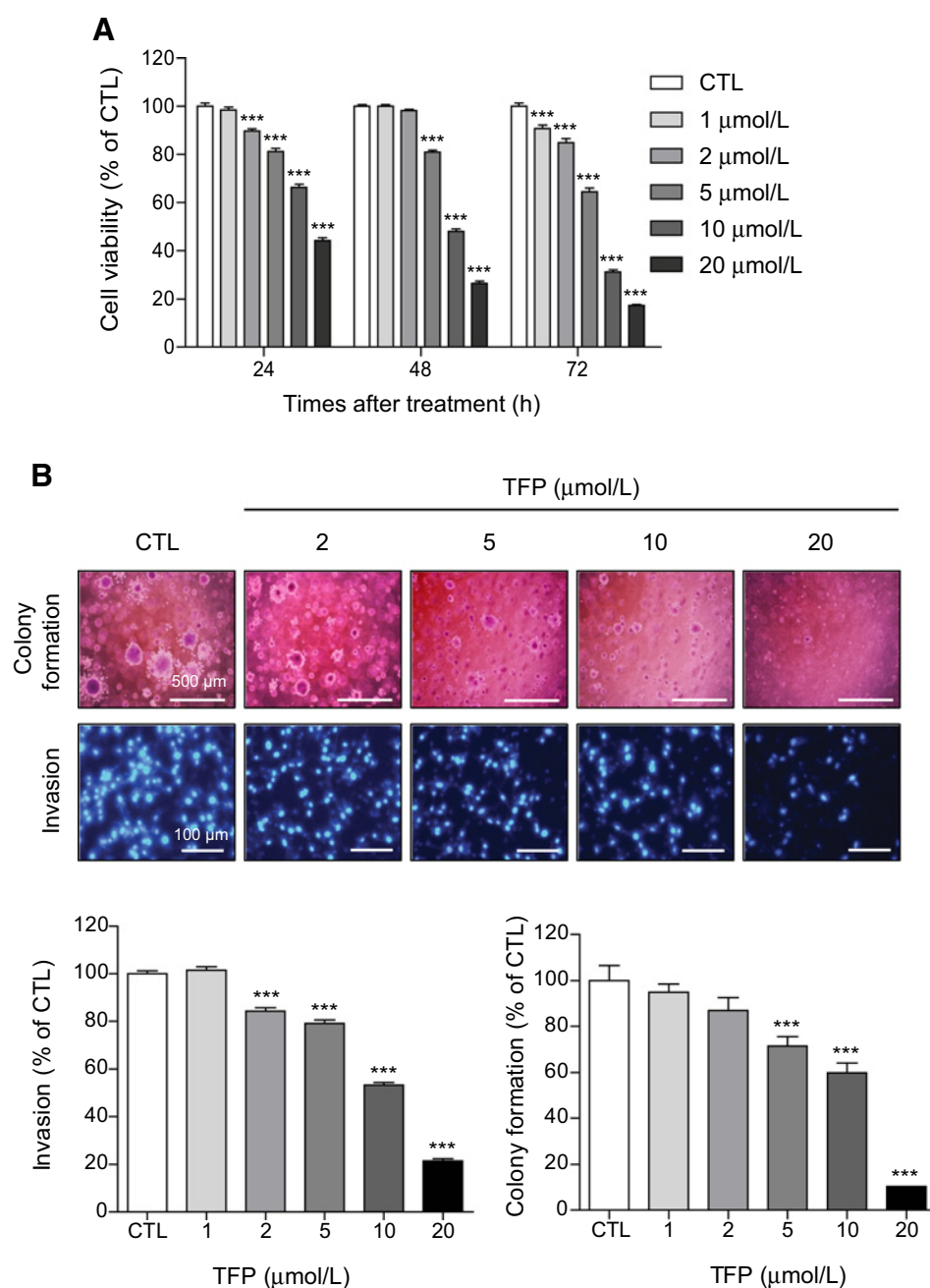
Figure 1.
TFP inhibits survival, colony formation, and invasion of U87MG glioblastoma cells. **A,** U87MG cells were treated with TFP at the indicated concentration for 24, 48, and 72 hours. CTL, control. MTT assay was used to determine inhibitory effects of TFP on U87MG cell proliferation. Percent cell viability is presented as mean $\pm$ SEM ($n = 16$). Asterisk (*), a significant difference determined by one-way ANOVA (***, $P < 0.001$). **B,** TFP effect on anchorage-independent growth and invasion of U87MG cells was tested by colony formation assay and Matrigel cell invasion assay, respectively. U87MG cells were treated with TFP at the indicated concentration for 2 weeks in colony formation assay, and for 24 hours in Matrigel cell invasion assay. TFP contained media was changed to fresh one in every 4 days. After 2 weeks, colonies were stained with 0.05% cresyl violet and photographed. All photographs were taken at a magnification of ×320 (top). Graph showed percentage of colonies and invasive cells, respectively (bottom). Asterisk indicates a significant difference determined by one-way ANOVA (***, $P < 0.001$).

from the autopsy showed that the lung metastasis was observed in the control group (71.4%, 4/7 mice) but not in the TFP-treated group (0%, 0/7 mice; Fig. 2D). Consistent with this result, H&E staining also showed that there was no lung metastasis in TFP-treated group compared with control in the skin xenograft model (Fig. 2D).
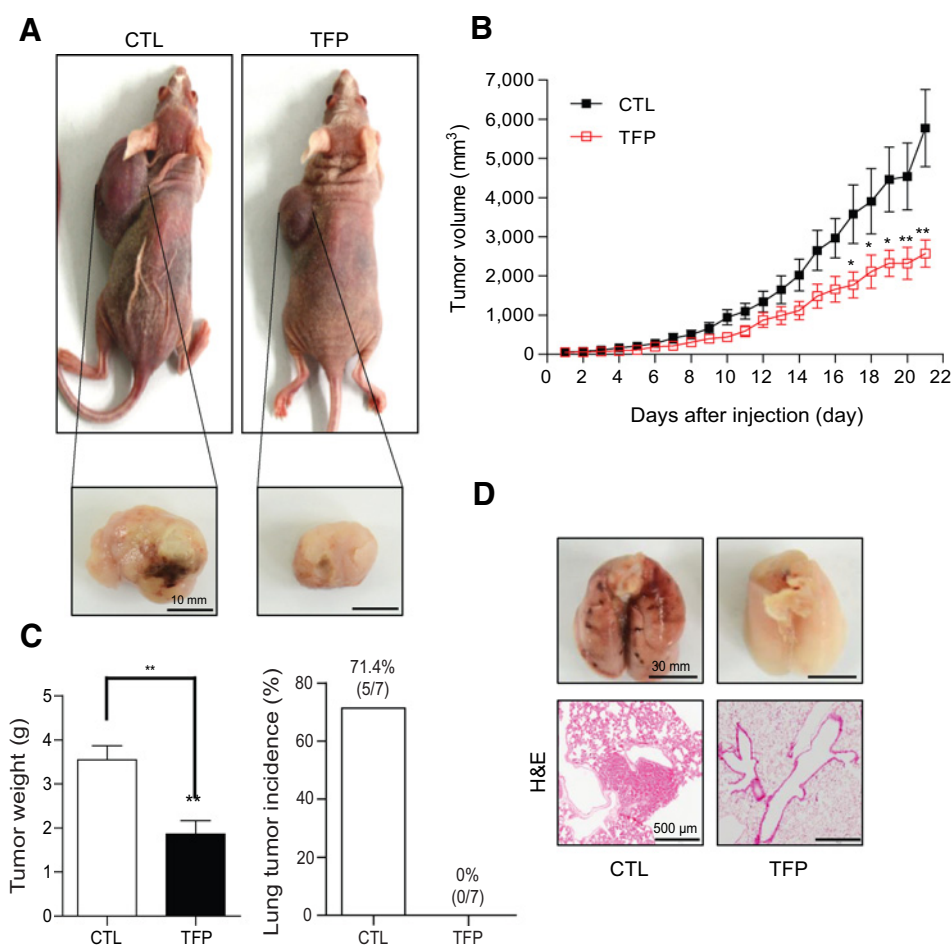
TFP induces robust intracellular Ca^{2+} increase in glioblastoma cells by Ca^{2+} release from ER

Intracellular Ca^{2+} is an important signal for gene expression, motility, differentiation, and survival of glioblastoma cells. In our previous study, we demonstrated that caffeine blocks the Ca^{2+} release from the IP$_3$R subtype 3, decreases the invasion of

glioblastoma cells, and finally increases the survival of the mouse implanted with glioblastoma tumor (5). Therefore, we examined whether TFP is associated with the intracellular Ca^{2+} in glioblastoma cells using Ca^{2+} indicator dye, Fura-2-AM. Unexpectedly, TFP application to cultured U87MG cells induced an increase in cytoplasmic Ca^{2+} in the U87MG cells concentration dependently (Fig. 3A). This effect of Ca^{2+} increase in U87MG cells by TFP is opposite to the effect of Ca^{2+} inhibition by caffeine, yet both TFP and caffeine showed inhibitory effect on invasion and proliferation, suggesting that not only inhibiting intracellular Ca^{2+} increase but also increasing intracellular Ca^{2+} is critical for blocking glioblastoma cell growth and invasion.

Figure 2.
TFP inhibits U87MG tumor growth and metastasis in *in vivo* skin xenograft model. **A,** U87MG cells (3×10^6) were injected subcutaneously into the right flank of athymic mice (BALB/c nu/nu) and induced tumors. **B,** Effect of TFP (5 mg/kg/day) on the volume of tumor in *in vivo* skin xenograft model during 21 days [untreated control (CTL) $n = 7$, TFP treated $n = 9$]. Asterisk indicates a significant difference determined by unpaired two-tailed t test (*, $P < 0.05$; **, $P < 0.01$). **C,** Effect of TFP (5 mg/kg/day) on the weight of tumor in *in vivo* skin xenograft model at day 21 (untreated control $n = 7$, TFP treated $n = 9$). Asterisk indicates a significant difference determined by unpaired two-tailed t test (**, $P < 0.01$). **D,** Photograph showing the lung organs of U87MG cell xenograft model (top). H&E staining of lung tissue in 0.9% saline-treated control group and TFP-treated group.

To determine whether TFP-induced Ca^{2+} increase is caused by Ca^{2+} entry from extracellular space or Ca^{2+} release from intracellular stores, such as endoplasmic reticulum (ER), we performed Ca^{2+} imaging experiments under three conditions: normal 2 mmol/L Ca^{2+}–containing bath condition, Ca^{2+}-free bath condition; and thapsigargin (TG) treatment in Ca^{2+}-free bath condition. We firstly treated with 100 μmol/L TFP in 2 mmol/L Ca^{2+} bath solution and found a robust Ca^{2+} increase in U87MG cells like in Fig. 3A. Next, we removed Ca^{2+} entry from outside by using Ca^{2+}-free bath solution and found that 100 μmol/L TFP also induced Ca^{2+} increase in U87MG cells, although there was about 32% decrease of Ca^{2+} peak ratio compared with 2 mmol/L calcium–containing bath condition (Fig. 3B). Next, we depleted Ca^{2+} stores by treating with TG in Ca^{2+}-free bath solution and found that there was almost no calcium increase by 100 μmol/L TFP (Fig. 3B). These results indicate that ER Ca^{2+} release is the major initiating contributor to TFP-induced Ca^{2+} increase in glioblastoma cells.

The molecular mechanism of Ca^{2+} increase and antiglioblastoma effect by TFP

It has been reported that Ca^{2+}-bound CaM is known to inhibit the opening of Ca^{2+} release channel, IP$_3$R (23). In addition, TFP binding to CaM is reported to cause conformational change and functional loss of CaM (22). Therefore, we hypothesized that the molecular mechanism of TFP-induced Ca^{2+} response might involve IP$_3$R and CaM. We first examined whether TFP-induced Ca^{2+} response is affected by gene silencing of *IP$_3$R* in U87MG cells. We confirmed the knockdown efficiency of each *IP$_3$R* subtype 1, 2, and 3 shRNA by Western blot analysis (Supplementary Fig. S3A). Gene silencing of *IP$_3$R* subtype 1 or 2 by lentivirus carrying *IP$_3$R1* or *IP$_3$R2* shRNA resulted in a significant decrease in 100 μmol/L TFP-induced Ca^{2+} response compared with that of the control scrambled shRNA in U87MG cells (Fig. 4A). However, Ca^{2+} response by 100 μmol/L TFP in *IP$_3$R3* shRNA-infected U87MG cells was not different with that in scrambled shRNA-infected U87MG cells (Fig. 4A). These results showed that TFP-induced Ca^{2+} increase in glioblastoma cells is mediated by opening of IP$_3$R subtype 1 and 2, but not subtype 3.

Next, we checked whether the IP$_3$R1 and 2 can affect glioblastoma cell viability by silencing the *IP$_3$R1* or *2* gene by shRNA for *IP$_3$R1* or *2* in cell counting assay (Fig. 4B). We observed that surviving U87MG cell number in *IP$_3$R1* or *IP$_3$R2* shRNA-infected U87MG cells was significantly more than that in scrambled shRNA-infected U87MG cells after 5 μmol/L TFP treatment (Fig. 4B), indicating that IP$_3$R1 and 2 contribute to the TFP-induced glioblastoma cell death. However, cell number in *IP$_3$R3* shRNA-infected U87MG cells did not differ with that in scrambled shRNA-infected U87MG cells after 5 μmol/L TFP treatment (Fig. 4B), implying that IP$_3$R3 did not contribute to the antiglioblastoma effect by TFP. This was also confirmed with GBL28 by *IP$_3$R1* shRNA, which showed most effect on U87MG cell viability
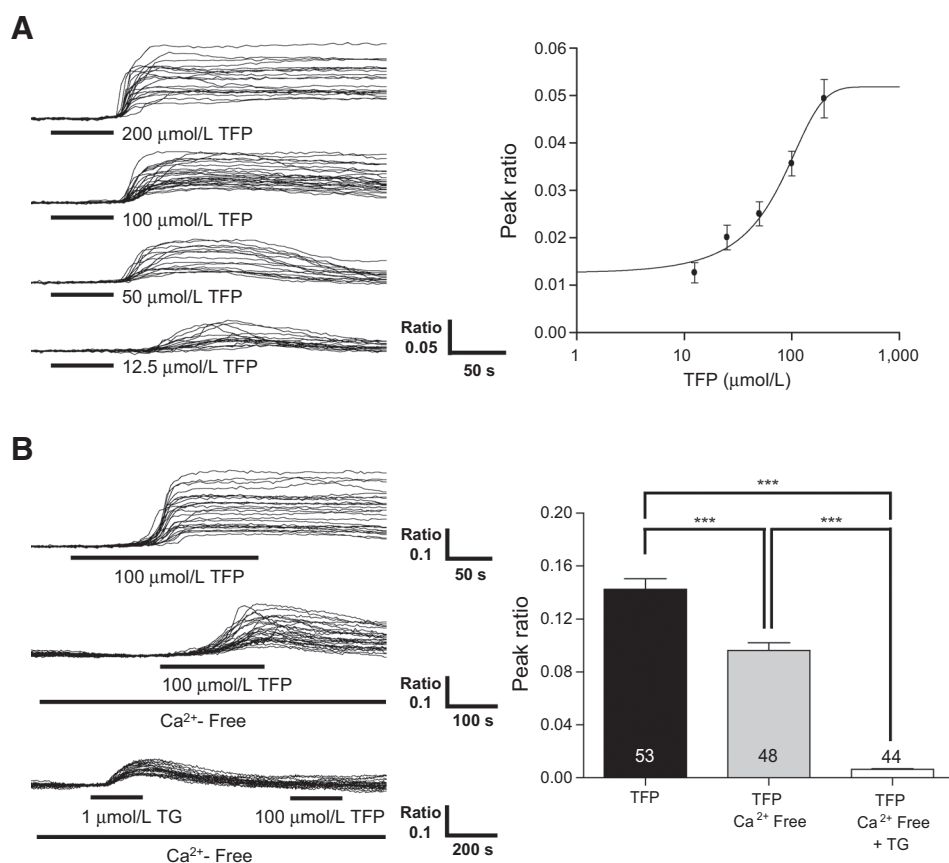
Figure 3.
TFP induces intracellular Ca^{2+} increase by Ca^{2+} release from ER. **A,** Traces from Ca^{2+} imaging recordings performed in U87MG cells in the presence of indicated TFP concentration. Each trace represents a Ca^{2+} response in one cell. Black horizontal bars, time and duration of TFP application (left). Dose–response curve from peak ratio of Ca^{2+} imaging trace corresponding to each TFP concentration with an EC_{50} of 56.8 µmol/L (right). **B,** Traces from Ca^{2+} imaging recordings performed in U87MG cells in the three conditions: in 2 mmol/L Ca^{2+} bath, in Ca^{2+}-free bath, and in Ca^{2+}-free bath with TG (left). Analysis of Fura-2-AM peak ratio from each of the three conditions (right). Black horizontal bars, time and duration of TFP application. Asterisk indicates a significant difference determined by unpaired two-tailed t test (***, $P < 0.001$).

(Supplementary Fig. S3B). Result of cell counting assay using GBL28 cells (Supplementary Fig. S3B) was consistent with the result in U87MG cells (Fig. 4B). On the basis of these results, we conclude that antiglioblastoma effect by TFP is mainly mediated by IP_3R subtype 1.

We next investigated whether CaM is associated with TFP-induced Ca^{2+} increase in U87MG cells. First, the expression level of CaM subtypes was measured by real-time PCR in GBL28 cells and NSCs as control (Fig. 4C). We found that CaM2 is expressed at a much higher level than other CaM subtypes in GBL28 cells (Fig. 4C). Moreover, the expression level of CaM2 in GBL28 cells was up to 2-fold higher than that in NSCs (Fig. 4C). Then, we tested the involvement of CaM2 in TFP-induced Ca^{2+} response by CaM2 shRNA-infected U87MG cells. We found that CaM2 shRNA decreased approximately 70% of the Ca^{2+} release by 100 µmol/L TFP compared with scrambled shRNA (Fig. 4D). To test whether the reduction in TFP-induced Ca^{2+} response in U87MG cells is caused by the specific gene silencing of CaM2, we coinfected wild-type CaM2 (sh-insensitive), which has mutations in CaM2 shRNA target sequence, so that it is no longer sensitive to CaM2 shRNA, along with CaM2 shRNA. Under this condition, Ca^{2+} response was rescued to the control scrambled shRNA condition (Fig. 4D). In addition, we tested whether the physical interaction between TFP and CaM is critical for TFP-induced Ca^{2+} increase by introducing a Q to A mutation at 120 residue in CaM2 (CaM2-Q120A), which is known to be the critical amino acid residue for TFP binding to CaM (22). The Q120A mutation was introduced in the CaM2 gene that contains CaM2 shRNA-insensitive sequence so that when coinfected with CaM2 shRNA,

CaM2-Q120A would not be able to interact with TFP in the absence of the endogenous CaM2. We observed that the TFP-induced Ca^{2+} response was not rescued by CaM2-Q120A after infected with CaM2 shRNA and CaM2-Q120A, which has TFP-binding mutant CaM2 and CaM2 shRNA-insensitive sequence (Fig. 4D). On the basis of these results, we concluded that TFP opens the IP_3R subtype 1 and 2 indirectly by binding to CaM2 and subsequently causing a conformational change of CaM2 that results in disinhibition (or relief of inhibition) of IP_3R, leading to opening of IP_3R.

Inhibitory effect of TFP in cell viability is specific to GBL cells, but not NSCs

Next, we examined whether the effect of TFP in cell viability is cell-type specific. We performed MTT assay and tested the inhibitory effect of TFP in GBL cells and NSC viability. As shown in Fig. 5A, concentrations higher than 5 µmol/L TFP showed a significant toxicity for NSCs, whereas concentrations higher than 2 µmol/L TFP showed a significant toxicity for GBL28 cells (Fig. 5A). Furthermore, cell viability of NSCs decreased only about 10% at 10 µmol/L TFP, whereas GBL28 cells showed 40% decrease in cell viability at the same concentration (Fig. 5A). In addition, we found that cell viability of other GBL12, GBL13, GBL15, GBL30, GBL227, and GBL232 was significantly decreased compared with NSCs (Supplementary Fig. S4). These results indicated that TFP can affect both types of cell, but glioblastoma cells show much higher sensitivity to TFP.

To see whether the heightened sensitivity to TFP in GBL cells is due to an enhanced Ca^{2+} increase, we compared the TFP-induced
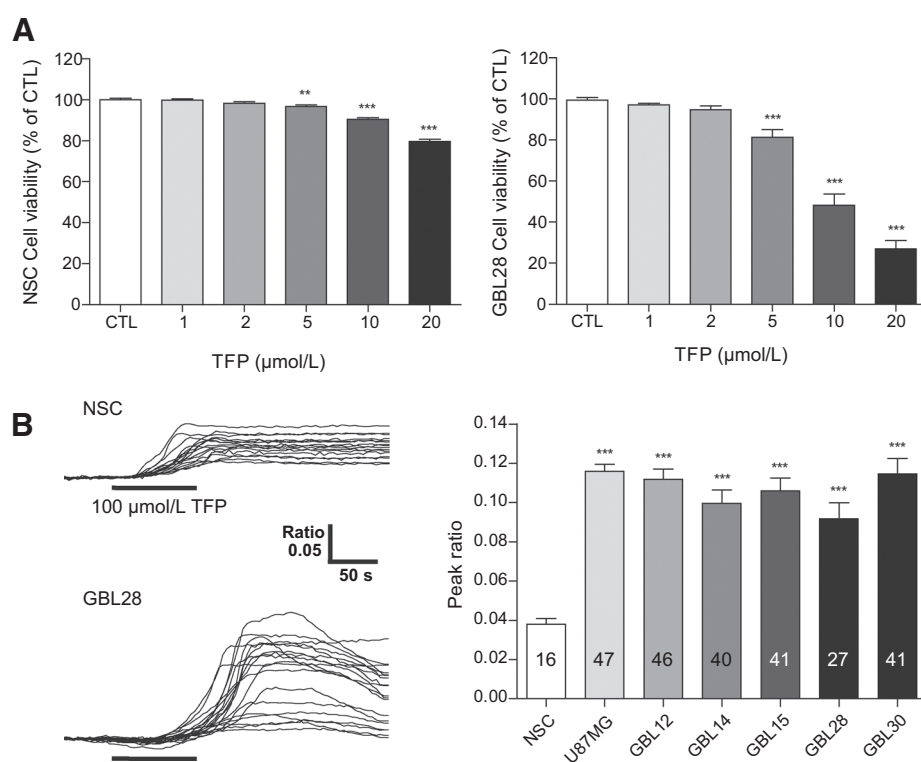
Figure 4.
IP$_3$R1, 2, and CaM2 are important for antiglioblastoma effect and inducing Ca^{2+} increase by TFP in glioblastoma cells. **A,** Ca^{2+} responses on U87MG cells infected with scrambled shRNA, IP$_3$R1 or R2, or R1/R2 or R3 shRNA in each condition (left). Black horizontal bars, time and duration of TFP application. Bar graph shows analysis of Fura-2-AM peak ratio from all conditions (right). Asterisk indicates a significant difference determined by unpaired two-tailed t test (*, P < 0.05; ***, P < 0.001); n.s., nonsignificant difference (P > 0.05). **B,** Cell counting was used to determine inhibitory effects of TFP on scrambled shRNA and IP$_3$R shRNAs-infected U87MG cell viability. Asterisk indicates a significant difference determined by unpaired two-tailed t test (**, P < 0.01; ***, P < 0.001); n.s., nonsignificant difference (P > 0.05). **C,** Fold expression of CaM mRNA was measured by qRT-PCR in GBL cells and NSCs. **D,** Ca^{2+} responses on U87MG cells infected with scrambled shRNA, CaM2 shRNA, CaM2 gene (insensitive to CaM2 shRNA), and TFP-binding mutant CaM2-Q120A (insensitive to CaM2 shRNA) in several combination conditions as indicated (left). Black horizontal bars, time and duration of TFP application. Bar graph shows analysis of Fura-2-AM peak ratio from each condition (right). Asterisk indicates a significant difference determined by unpaired two-tailed t test (***, P < 0.001); n.s., nonsignificant difference (P > 0.05).
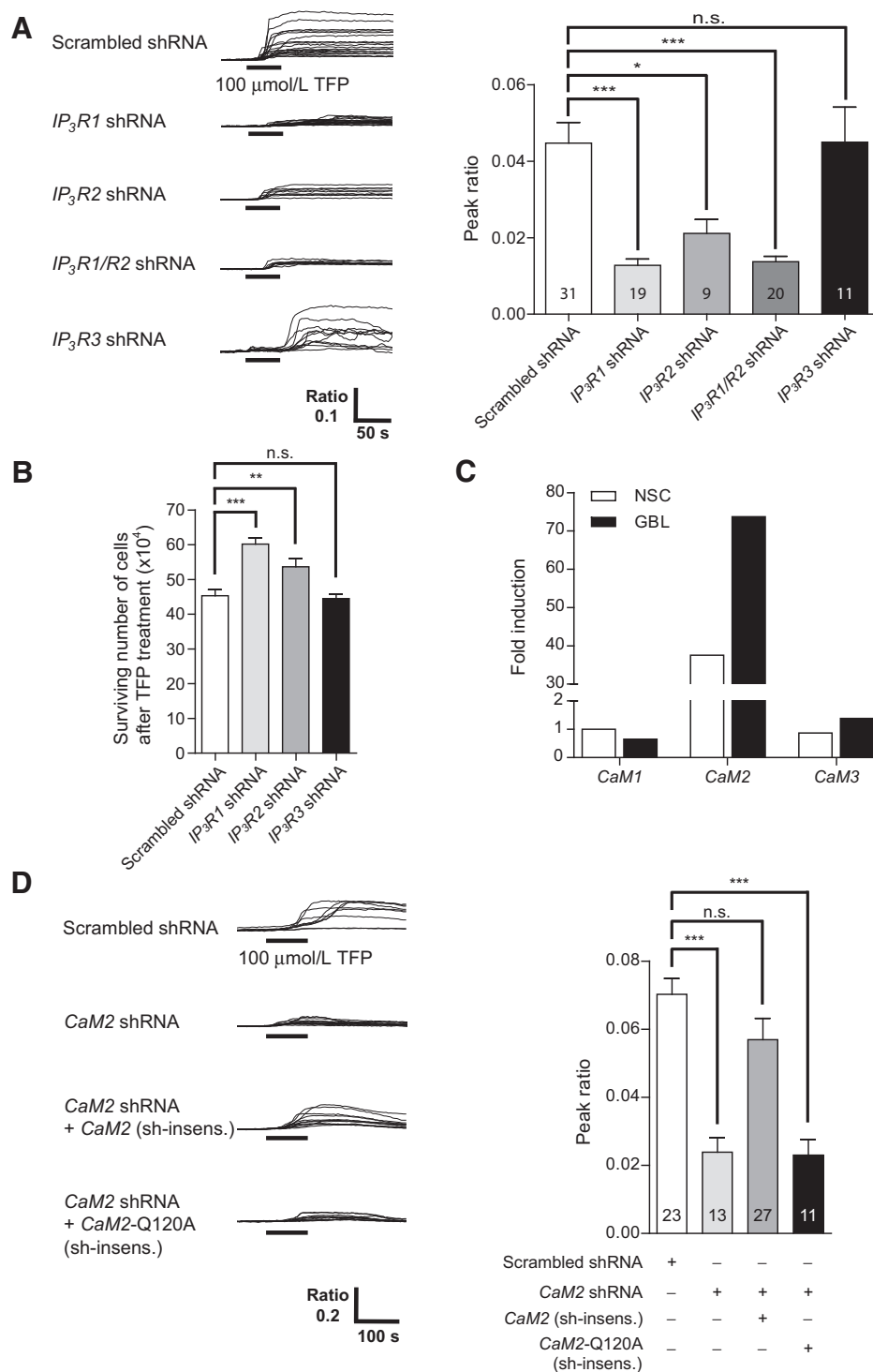
Ca^{2+} increase in NSCs, U87MG cells, and several GBL cells (GBL12, GBL14, GBL15, GBL28, and GBL30). Consistent with MTT assay results, TFP-induced Ca^{2+} response in GBL cells (GBL12, GBL14, GBL15, GBL28, and GBL30) and U87MG cells was significantly higher than NSCs Ca^{2+} response (Fig. 5B). On the basis of these results, we concluded that TFP is more effective and potent in glioblastoma cells than in normal cells.

TFP inhibits glioblastoma growth on the orthotopic xenograft brain tumor

To further test the potential therapeutic effect of TFP on glioblastoma, we examined the inhibitory effects of TFP on glioblastoma growth in orthotopic xenograft mice. We implanted U87MG cells into the left frontal lobe of athymic mice (BALB/c nu/nu) by intracranial injections. TFP (10 mg/kg/day) was given

A

B

Figure 5.
TFP has a more toxic effect to several GBL cells than NSCs. **A,** MTT assay was used to determine inhibitory effects of TFP on NSCs (left) and GBL28 cells (right) viability. CTL, control. Both cells were treated with TFP at the indicated concentration for 24 hours. Asterisk indicates a significant difference determined by one-way ANOVA (**, $P < 0.01$; ***, $P < 0.001$). **B,** Traces from Ca^{2+} imaging recordings performed in NSCs, U87MG, GBL12, GBL14, GBL15, GBL28, and GBL30 in response to 100 µmol/L TFP. Each trace represents a Ca^{2+} response in NSCs and GBL28 cells (left). Black horizontal bars, time and duration of TFP application. Bar graph shows analysis of Fura-2-AM peak ratio from each condition (right). Asterisk indicates a significant difference determined by unpaired two-tailed t test (***, $P < 0.001$).

as an intraperitoneal injection 3 days after implantation, and drug administration schedule was same as the skin xenograft model. Mice were monitored daily for general appearance, behavioral changes, and neurologic deficits. Mice were sacrificed when moribund. Mouse brain was stained with H&E to visualize and measure the tumor size in the brain (Fig. 6A). We found that TFP treatment reduced over 75% of the tumor volume compared with control mice (Fig. 6B). However, in the survival test in orthotopic xenograft mice, TFP only modestly extended the survival time compared with the control group (Fig. 6C). From these results, we concluded that TFP shows a strong inhibitory effect on glioblastoma growth *in vivo* but, for unknown reasons, only modestly extends the survival time in mice.

Discussion

We investigated here the therapeutic potential of TFP on glioblastoma and underlying detailed molecular and cellular mechanisms of TFP action by using both *in vitro* and *in vivo* assays. In summary, TFP suppressed proliferation (Fig. 1A), migration (Fig. 1B), and invasion (Fig. 1B) of glioblastoma cells in several *in vitro* assays. Furthermore, tumor size and weight in *in vivo* skin xenograft model (Fig. 2) and in orthotopic brain xenograft model (Fig. 6) of glioblastoma were markedly decreased by TFP treatment. We found that the glioblastoma-specific cytotoxic effect of TFP is linked to intracellular Ca^{2+} increase by release of Ca^{2+} from ER through IP_3Rs. Among the three types of IP_3R, by using IP_3R1, 2, and 3 shRNA, we identified that IP_3R subtype 1 and 2 are the major contributors of TFP-induced Ca^{2+} increase in glioblastoma (Fig. 4A). Furthermore, we identified that activation of IP_3R1 by TFP can be critical for the cell viability of GBL cells (Fig. 4B). TFP-induced Ca^{2+} increase is also associated with CaM, which is

involved in modulation of Ca^{2+} signaling through interaction with Ca^{2+} (28, 29). We found that CaM2 is the major type among three types of CaM and is overexpressed in GBL cell lines compared with NSCs (Fig. 4C). Moreover, the gene silencing of *CaM2* by shRNA reduced TFP-induced Ca^{2+} increase significantly (Fig. 4D).

Regulation of IP_3R opening has been investigated in previous studies: one of the well-known mechanisms is the regulation of IP_3R by CaM and Ca^{2+} (24, 25). According to this mechanism, IP_3R is blocked by Ca^{2+}/CaM complex, which binds to the N-terminal domain of IP_3R under normal condition (24, 25). TFP, also known as a CaM antagonist, binds to CaM and induces conformational change and functional loss of CaM (22). On the basis of these well-known mechanisms, we hypothesized that TFP inhibits CaM function, which normally inhibits IP_3R opening, and subsequently induces robust Ca^{2+} release from ER by disinhibiting (or relieving the inhibition of) IP_3R (Fig. 6D). In fact, when we used CaM2 shRNA and CaM2-Q120A, which has a mutation in TFP-binding site with *CaM2* shRNA-insensitive sequence, TFP-induced Ca^{2+} increase was impaired (Fig. 4D), supporting our hypothesis.

In our previous study, we demonstrated that caffeine inhibits intracellular Ca^{2+} increase by IP_3R3, whose expression level is increased in glioblastoma cells compared with normal glial cells (5). We further demonstrated that caffeine blocks glioblastoma migration, invasion *in vitro*, and extends survival in the xenograft mouse model of glioblastoma by inhibiting IP_3R3-mediated Ca^{2+} release from ER (5). These results suggested that inhibiting the Ca^{2+} signaling could suppress the aggressive motility and invasiveness of glioblastoma cells (5). On the other hand, TFP increased intracellular Ca^{2+} in glioblastoma cells by inducing opening of IP_3R1 and 2. Consequently, TFP inhibited glioblastoma migration and invasion *in vitro* and *in vivo*. These results
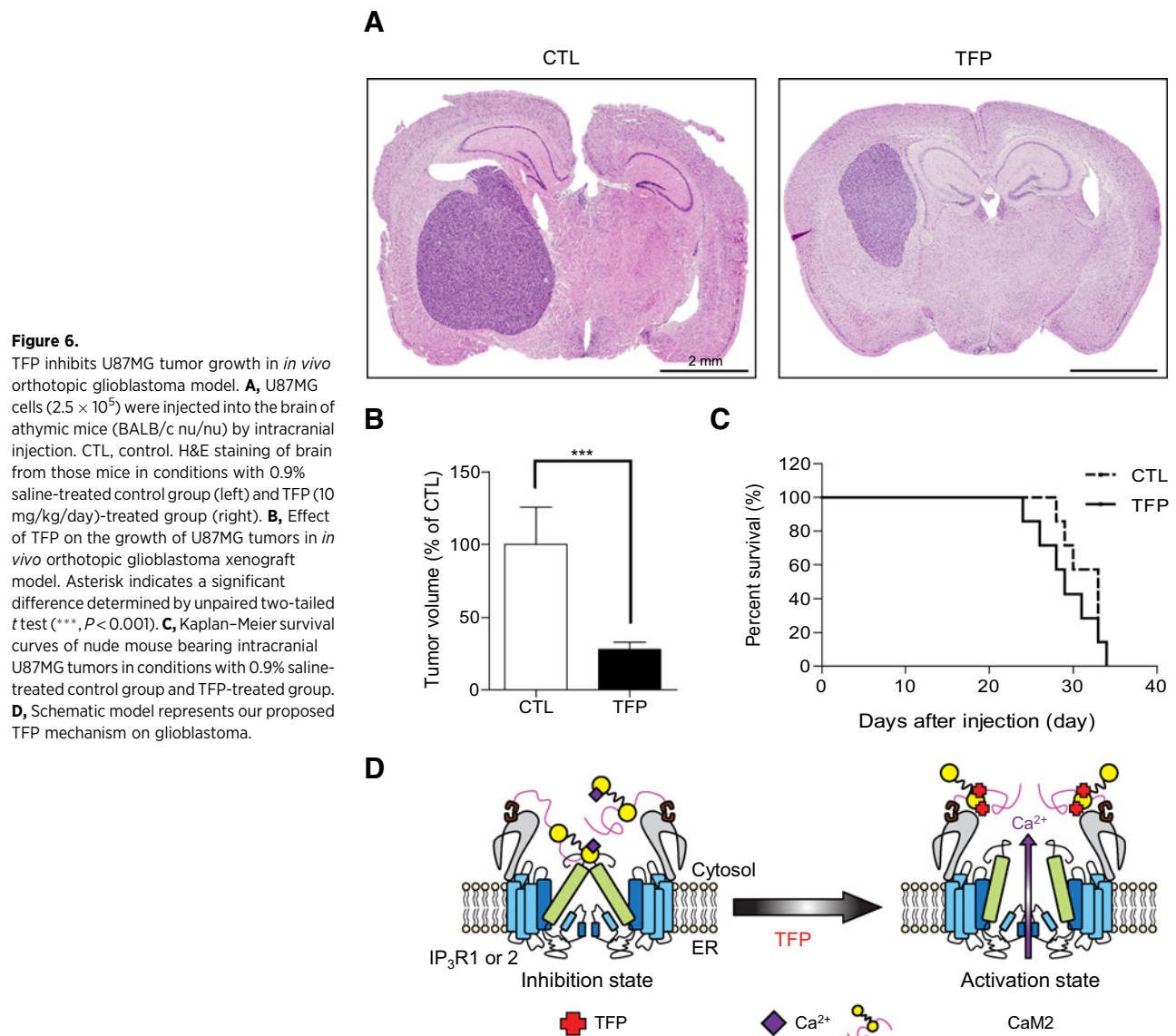
Figure 6.
TFP inhibits U87MG tumor growth in *in vivo* orthotopic glioblastoma model. **A,** U87MG cells (2.5×10^5) were injected into the brain of athymic mice (BALB/c nu/nu) by intracranial injection. CTL, control. H&E staining of brain from those mice in conditions with 0.9% saline-treated control group (left) and TFP (10 mg/kg/day)-treated group (right). **B,** Effect of TFP on the growth of U87MG tumors in *in vivo* orthotopic glioblastoma xenograft model. Asterisk indicates a significant difference determined by unpaired two-tailed t test (***, $P < 0.001$). **C,** Kaplan–Meier survival curves of nude mouse bearing intracranial U87MG tumors in conditions with 0.9% saline-treated control group and TFP-treated group. **D,** Schematic model represents our proposed TFP mechanism on glioblastoma.

indicated that aberrant increase in the Ca^{2+} signaling pathway could also inhibit the motile and invasive nature of glioblastoma cells. Intracellular Ca^{2+} is important for the regulation of various intracellular events, such as metabolism, gene expression, and survival, and therefore, it is highly regulated (30). If Ca^{2+} homeostasis is broken, regardless of overload or lack of intracellular Ca^{2+}, cells experience adverse effects, such as cell death. Therefore, both caffeine and TFP could have a similar inhibitory effect on glioblastoma growth and invasion by either inhibiting or increasing intracellular Ca^{2+}, respectively.

The practical dose of TFP for mental disorder therapy is usually 10 mg/day for adult (bodyweight, 60 kg) and is adjusted according to the degree of the side effects (13). A dose of 100 to 150 mg/day is also used in a particular case of patients (13). In the current study, a dose of TFP at 5 mg/kg was used for skin xenograft model (Fig. 2), and a dose of 10 mg/kg was used for orthotopic brain xenograft model (Fig. 6). The dose of TFP used for animal experiments was much higher than that for patients

with a mental disorder. Therefore, we were concerned about potential side effects of TFP experimental animals, such as Parkinsonism and extrapyramidal side effect (EPS) as described previously (12). However, at a dose of 5 mg or 10 mg/kg/day in our animal experiments, very little signs of side effects were observed, and even if EPS was observed in a few cases, it disappeared within a few minutes. Therefore, we concluded that at the current doses, there might be very few side effects by TFP.

Recently, numerous studies have focused on drug repositioning, namely discovering new indications for existing drugs for cancer therapy (31–33). Repositioning of currently used medications can be time saving and money saving in terms of research funding. It has been recently proposed that new glioblastoma treatment approach using nine drugs that are currently marketed for cytotoxic chemotherapy along with temozolomide could have a therapeutic effect in recurrent glioblastoma. The nine adjuvant drug regimen, so called coordinated undermining of survival paths (CUSP9), includes aprepitant, artesunate, auranofin,

captopril, celecoxib, disulfiram, itraconazole, ritonavir, and sertraline, augmenting continuous low-dose temozolomide (34, 35). It has been reported that glioblastoma cell viability was markedly decreased in CUSP9-treated cells compared with temozolomide alone (35). In addition to CUSP9, here, we propose another antiglioblastoma drug TFP that satisfies the concept of drug repositioning. It has been reported that TFP, a well-known antipsychotic drug, has shown anticancer effect in several cancer cell lines, such as lung cancer, hepatocellular carcinoma, and T-cell lymphoma (14–21). Moreover, TFP was viewed as a potential reagent for glioblastoma treatment due to its safety and high permeability of blood–brain barrier (36). In this study, we identified a new use of TFP for glioblastoma therapy and delineated detailed molecular and cellular mechanism of TFP action on glioblastoma. Our study proposes TFP as a valuable therapeutic drug for glioblastoma and also calls for future development of more effective TFP derivatives.

Disclosure of Potential Conflicts of Interest

No potential conflicts of interest were disclosed.

Authors' Contributions

Conception and design: S. Kang, J.M. Lee, S.H. Paek, E.J. Roh, S.S. Kang
Development of methodology: J. Hong, J. Choi, S.S. Kang
Acquisition of data (provided animals, acquired and managed patients, provided facilities, etc.): S. Kang, H.E. Moon, S.H. Paek, C.J. Lee, S.S. Kang
Analysis and interpretation of data (e.g., statistical analysis, biostatistics, computational analysis): J. Hong, J.M. Lee, J. Choi, S.H. Paek, C.J. Lee, S.S. Kang
Writing, review, and/or revision of the manuscript: S. Kang, J.M. Lee, N.A. Yoon, C.J. Lee, S.S. Kang

References

1. Stupp R, Hegi ME, Mason WP, van den Bent MJ, Taphoorn MJ, Janzer RC, et al. Effects of radiotherapy with concomitant and adjuvant temozolomide versus radiotherapy alone on survival in glioblastoma in a randomised phase III study: 5-year analysis of the EORTC-NCIC trial. Lancet Oncol 2009;10:459–66.
2. Rao JS. Molecular mechanisms of glioma invasiveness: the role of proteases. Nat Rev Cancer 2003;3:489–501.
3. Nakada M, Nakada S, Demuth T, Tran NL, Hoelzinger DB, Berens ME. Molecular targets of glioma invasion. Cell Mol Life Sci 2007; 64:458–78.
4. Ostrom QT, Gittleman H, Fulop J, Liu M, Blanda R, Kromer C, et al. CBTRUS statistical report: primary brain and central nervous system tumors diagnosed in the United States in 2008-2012. Neuro Oncol 2015;17:iv1–iv62.
5. Kang SS, Han KS, Ku BM, Lee YK, Hong J, Shin HY, et al. Caffeine-mediated inhibition of calcium release channel inositol 1,4,5-trisphosphate receptor subtype 3 blocks glioblastoma invasion and extends survival. Cancer Res 2010;70:1173–83.
6. Friedman HS, Kerby T, Calvert H. Temozolomide and treatment of malignant glioma. Clin Cancer Res 2000;6:2585–97.
7. Komotar RJ, Otten ML, Moise G, Connolly ESJr.Radiotherapy plus concomitant and adjuvant temozolomide for glioblastoma-a critical review. Clin Med Oncol 2008;2:421–2.
8. Dalton SO, Johansen C, Poulsen AH, Norgaard M, Sorensen HT, McLaughlin JK, et al. Cancer risk among users of neuroleptic medication: a population-based cohort study. Br J Cancer 2006;95:934–9.
9. Chou FH, Tsai KY, Su CY, Lee CC. The incidence and relative risk factors for developing cancer among patients with schizophrenia: a nine-year follow-up study. Schizophr Res 2011;129:97–103.
10. Nordenberg J, Fenig E, Landau M, Weizman R, Weizman A. Effects of psychotropic drugs on cell proliferation and differentiation. Biochem Pharmacol 1999;58:1229–36.
11. Shin SY, Lee KS, Choi YK, Lim HJ, Lee HG, Lim Y, et al. The antipsychotic agent chlorpromazine induces autophagic cell death by inhibiting the Akt/mTOR pathway in human U-87MG glioma cells. Carcinogenesis 2013;34:2080–9.
12. Kau TR, Schroeder F, Ramaswamy S, Wojciechowski CL, Zhao JJ, Roberts TM, et al. A chemical genetic screen identifies inhibitors of regulated nuclear export of a Forkhead transcription factor in PTEN-deficient tumor cells. Cancer Cell 2003;4:463–76.
13. Marques LO, Lima MS, Soares BG. Trifluoperazine for schizophrenia. Cochrane Database Syst Rev 2004;1:CD003545.
14. Frankfurt OS, Sugarbaker EV, Robb JA, Villa L. Synergistic induction of apoptosis in breast cancer cells by tamoxifen and calmodulin inhibitors. Cancer Lett 1995;97:149–54.
15. Karmakar P, Natarajan AT, Poddar RK, Dasgupta UB. Induction of apoptosis by Phenothiazine derivatives in V79 cells. Toxicol Lett 2001;125:19–28.
16. Shin SY, Kim CG, Hong DD, Kim JH, Lee YH. Implication of Egr-1 in trifluoperazine-induced growth inhibition in human U87MG glioma cells. Exp Mol Med 2004;36:380–6.
17. Annabi B, Pilorget A, Bousquet-Gagnon N, Gingras D, Beliveau R. Calmodulin inhibitors trigger the proteolytic processing of membrane type-1 matrix metalloproteinase, but not its shedding in glioblastoma cells. Biochem J 2001;359:325–33.
18. Murren JR, Durivage HJ, Buzaid AC, Reiss M, Flynn SD, Carter D, et al. Trifluoperazine as a modulator of multidrug resistance in refractory breast cancer. Cancer Chemother Pharmacol 1996;38:65–70.
19. Schleuning M, Brumme V, Wilmanns W. Growth inhibition of human leukemic cell lines by the phenothiazine derivative fluphenazine. Anticancer Res 1993;13:599–602.
20. Yeh CT, Wu AT, Chang PM, Chen KY, Yang CN, Yang SC, et al. Trifluoperazine, an antipsychotic agent, inhibits cancer stem cell growth and

overcomes drug resistance of lung cancer. Am J Respir Crit Care Med 2012;186:1180–8.

21. Chen MH, Lin KJ, Yang WL, Kao YW, Chen TW, Chao SC, et al. Gene expression-based chemical genomics identifies heat-shock protein 90 inhibitors as potential therapeutic drugs in cholangiocarcinoma. Cancer 2013;119:293–303.

22. Vandonselaar M, Hickie RA, Quail JW, Delbaere LT. Trifluoperazine-induced conformational change in Ca(2+)-calmodulin. Nat Struct Biol 1994;1:795–801.

23. Michikawa T, Hirota J, Kawano S, Hiraoka M, Yamada M, Furuichi T, et al. Calmodulin mediates calcium-dependent inactivation of the cerebellar type 1 inositol 1,4,5-trisphosphate receptor. Neuron 1999;23:799–808.

24. Taylor CW, Laude AJ. IP3 receptors and their regulation by calmodulin and cytosolic Ca2+. Cell Calcium 2002;32:321–34.

25. Nadif Kasri N, Bultynck G, Sienaert I, Callewaert G, Erneux C, Missiaen L, et al. The role of calmodulin for inositol 1,4,5-trisphosphate receptor function. Biochim Biophys Acta 2002;1600:19–31.

26. Clapham DE. Calcium signaling. Cell 2007;131:1047–58.

27. Prevarskaya N, Skryma R, Shuba Y. Calcium in tumour metastasis: new roles for known actors. Nat Rev Cancer 2011;11:609–18.

28. Santella L. The role of calcium in the cell cycle: facts and hypotheses. Biochem Biophys Res Commun 1998;244:317–24.

29. Kahl CR, Means AR. Regulation of cell cycle progression by calcium/calmodulin-dependent pathways. Endocr Rev 2003;24:719–36.

30. Verkhratsky A, Orkand RK, Kettenmann H. Glial calcium: homeostasis and signaling function. Physiol Rev 1998;78:99–141.

31. Shin S, Lee S. Niacin as a drug repositioning candidate for hyperphosphatemia management in dialysis patients. Ther Clin Risk Manag 2014;10:875–83.

32. Ko EM, Walter P, Jackson A, Clark L, Franasiak J, Bolac C, et al. Metformin is associated with improved survival in endometrial cancer. Gynecol Oncol 2014;132:438–42.

33. Flahavan EM, Sharp L, Bennett K, Barron TI. A cohort study of digoxin exposure and mortality in men with prostate cancer. BJU Int 2014;113: 236–45.

34. Kast RE, Boockvar JA, Bruning A, Cappello F, Chang WW, Cvek B, et al. A conceptually new treatment approach for relapsed glioblastoma: coordinated undermining of survival paths with nine repurposed drugs (CUSP9) by the international initiative for accelerated improvement of glioblastoma care. Oncotarget 2013;4:502–30.

35. Kast RE, Karpel-Massler G, Halatsch ME. CUSP9* treatment protocol for recurrent glioblastoma: aprepitant, artesunate, auranofin, captopril, celecoxib, disulfiram, itraconazole, ritonavir, sertraline augmenting continuous low dose temozolomide. Oncotarget 2014;5: 8052–82.

36. Sangodkar J, Dhawan NS, Melville H, Singh VJ, Yuan E, Rana H, et al. Targeting the FOXO1/KLF6 axis regulates EGFR signaling and treatment response. J Clin Invest 2012;122:2637–51.